Progress In Electromagnetics Research M, Vol. 108, 53–63, 2022

Analysis of Electrically Low Profile Wideband Microwave Absorber for C Band Applications

Nitinkumar J. Bathani[1, *] and Jagdishkumar M. Rathod[2]

Abstract—In this paper, a wideband polarization-independent broad angular insensitive absorber is proposed with miniaturization novelty. A 12∗12 octagon element with parasitic elements interconnected by lumped resister has been fabricated on an FR4 structure with an air gap. Large air gap and lower thickness of substrate material as well as corner notched rectangular with octagonal shape causes the improvement of bandwidth. The proposed wideband absorber exhibits absorptivity above 90%. The same has been achieved from 2.84 GHz to 9.12 GHz with 6.27 GHz fractional bandwidth in TE and TM configurations with an angle from 0° to 30°. The design is $\lambda/6.67$ in size and $\lambda/3.33$ in thickness miniaturization at the highest cutoff wavelength. The outcome from the proposed model is highly promising and closely matches the simulated configuration. This design has a vital application in absorbing the signal from aircraft, missiles, submarines, satellites, and radar, termed stealth technology.

1. INTRODUCTION

Victor Veselego presented metamaterial property in 1968 [1], after which an extended number of designs have been proposed have been proposed. Metamaterial absorber comprises a metal part with single or multilayer dielectric material and has points of interest in slim thickness and wideband property. Landy et al. [2] presented the first microwave absorber. Microwave absorber is widely used in cloaking [3], RF harvesting [4], sensors, medical imaging, solar cells [5], chipless RFID tags [6], stealth technology [7], as well as satellite communication [8]. Metamaterial absorber has a property to change effective permittivity and permeability at a particular band of frequency such that intrinsic impedance of free space is coordinated with the input impedance of metamaterial absorber. Absorption in material is due to slightest reflection and without transmission. The proposed structure covers a full C band ranging from 4 to 8 GHz, called C band metamaterial absorber (CMMA). The Transmissive and reflective coefficients of an absorber are given as:

$$T(w) = S_{11}(w)^2 \tag{1}$$

$$R(w) = S_{21}(w)^2 \tag{2}$$

where $T(w)$ is the transmissive coefficient, and $R(w)$ is the reflective coefficient. The absorptivity of CMMA can be found by the following formula.

$$A(w)_{\text{CMMA}} = (1 - T(w) - R(w)) * 100\% \tag{3}$$

If CMMA comprises a ground plane, there is no transmission from the ground plane. Since MMA is a frequency-dependent device, a band of frequency shall be decided by CMMA in which it cannot reflect incident wave, thus its absorptivity increases, and CMMA can absorb the incident wave. The

Received 22 December 2021, Accepted 28 January 2022, Scheduled 9 February 2022

* Corresponding author: Nitinkumar J. Bathani (nitinbathani@gmail.com).

[1] Department of Electronics and Communication Engineering, Government Engineering College, Modasa, Gujarat, India. [2] Department of Electronics, Birla Vishvakarma Mahavidyalaya, Vallabh Vidyanagar, Gujarat, India.

bandwidth of CMMA can be increased by including more substrate materials [12, 21]. So radar cross-section (RCS) of respective CMMA is reduced by impedance matching at operating frequency band for the stealth application. The following formula can calculate normalized impedance.

$$Z_{\text{CMMA}} = \frac{1 + R(w)}{1 - R(w)} \tag{4}$$

At a specific frequency band, the reflection coefficient is minimized, which results in achieving normalized impedance close to unity representing perfect impedance matching and generates the highest absorptivity of CMMA. Wideband and thin substrate material is used for stealth application. Till now, so many designs of metamaterial absorbers have been analyzed, such as single band [2, 32], double band [9–13], triple band [14–17], quad-band [18, 19], wideband [20–25], polarization-independent [12, 26, 27, 33–36], oblique angle independent [28, 29], reconfigurable frequency selective absorber [30, 31].

In this article, we propose a structure with a unit cell that consists of an octagon element interconnected to four notched rectangular shapes at 90° with each other using a lumped resistor. The commercial high-frequency structure simulator (HFSS) optimizes the proposed structure, which is analyzed using the finite element method (FEM). Its equivalent electrical parameter can also represent the proposed structure for a specific frequency band. The numerically proposed structure can obtain less than 90% absorptivity from 2.84 GHz to 9.12 GHz. Thus, the operating bandwidth of the proposed structure is 105%. The proposed structure can also be simulated and analyzed in TE and TM polarizations at various oblique incident angles to confirm the polarization-insensitive structure. The same design has been fabricated in a 0.5 mm FR4 structure with an air gap. A perfect outcome has been accomplished among numerical analysis, simulated structure, and fabricated structure. The proposed structure is exceptionally used in the Radar application operated in the C band application.

In this article, Section 2 shows the unit cell design with all optimized parameters. Section 3 describes the absorption mechanism in the wider bandwidth of proposed CMMA. Section 4 presents the parametric study of various physical and electrical parameters to identify their effects. Fabricated structure with its complete estimation has been represented in Section 5. The work is concluded in Section 6.

2. CMMA UNIT CELL DESIGN

Metamaterial unit cell is designed by a 12×12 symmetrical structure with four resistors of $100\,\Omega$. Interspacing between the unit cells decides the capacitance of the proposed configuration. Octagon shape with the parasitic element as a rectangular notched shape, which is connected by the complete structure, is fabricated on a fragile 0.5 mm FR4 substrate consisting of relative dielectric constant ε_r of 4.4 as well as loss tangent ($\tan\delta$) of 0.02 with an air gap of 1 cm as shown in Fig. 1. The air gap, as well as notched rectangular shape, causes the enhancement of bandwidth. The parameters observed from optimization technique through HFSS of the proposed structure of the unit cell, in line with Fig. 1, is as follows.

$L1 = 7.8$ mm, $L2 = 4.4$ mm, $L3 = 2.2$ mm, $L4 = 1.3$ mm, $L5 = 3.2$ mm, and total length $L = 22$ mm. Four resistors of $100\,\Omega$ have been chosen to increase the absorption rate. The size of the unit cell is 2.2 cm, which is miniaturized to $\lambda/6.67$ at the lowest frequency. The thickness of proposed structure is 1.5 cm, which is miniaturized to $\lambda/3.33$ at the lowest frequency.

3. REASON FOR ABSORPTION IN WIDER BANDWIDTH

The proposed structure comprises a series of RLC circuits of copper structure having sizable current confinement, thus functioning as an inductor. Further, the coupling between the copper structures at the end of a unit cell generates capacitance. Multiple inductances have been generated using a variable length of metamaterial structure. As per the design of a 0.5 mm FR4 structure, a relative dielectric constant of the proposed structure is $\varepsilon_e = 4.33$. Theoretically, octagon perimeter causes the most minimal frequency, which is 1.28 cm, so it can deliver an effective wavelength of 5.12 cm (current length = $\lambda_e/4$), creating a 2.8 GHz frequency. It nearly matches a simulated result of 2.84 GHz. The

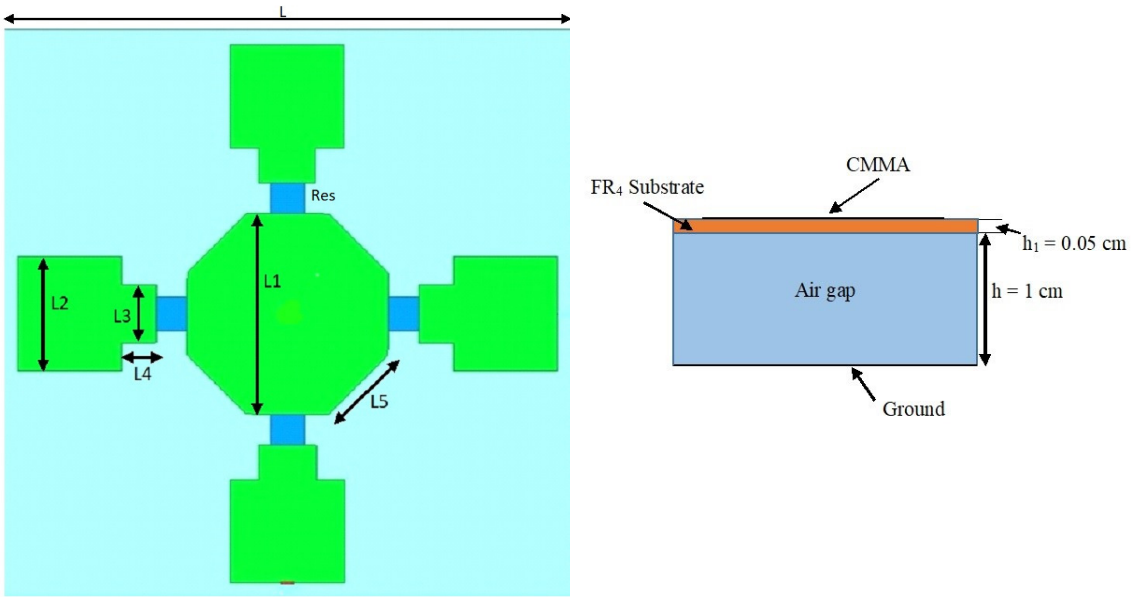

Figure 1. Simulated CMMA unit cell model, (a) front view, (b) side view.

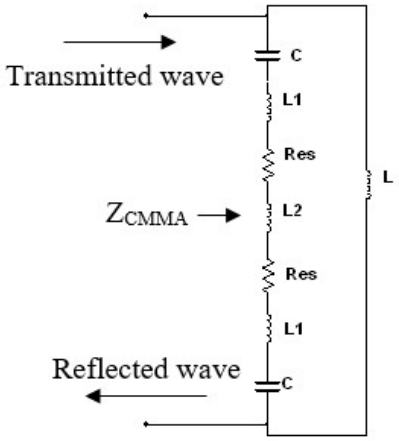

Figure 2. Equivalent (identical) circuit model of proposed CMMA.

highest frequency of the proposed structure can be exposed from the length of slotted parasitic elements, which is 4 mm, causing an effective wavelength of 16 mm, producing a frequency of 9 GHz, which can compare with the simulation frequency of 9.12 GHz. The equivalent circuit of projected CMMA configuration is presented in Fig. 2. The interconnection between unit cells produces capacitance C; multiple lengths of structure cause variable inductances with the same two resistances. Parallel inductance L can be created because of more substantial current confinement due to backed ground plane. Based on above, the formula suggested for evaluating normalized impedance for the proposed CMMA is as follows:

$$Z_{\text{CMMA}} = \frac{\left(\dfrac{2}{jwC} + 2 * jwL1 + 2 * Res + jwL2\right) \| (jwL)}{\eta} \tag{5}$$

So a complex variable of the simulated Z parameter is shown in Fig. 3, which is equivalent to the

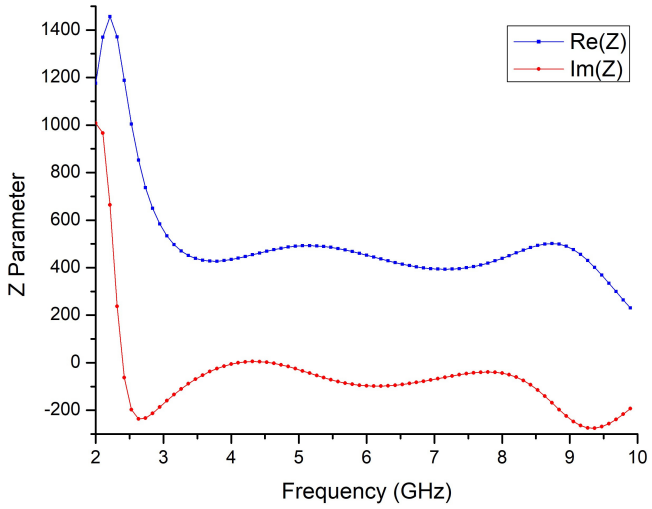

Figure 3. Z parameter of proposed CMMA.

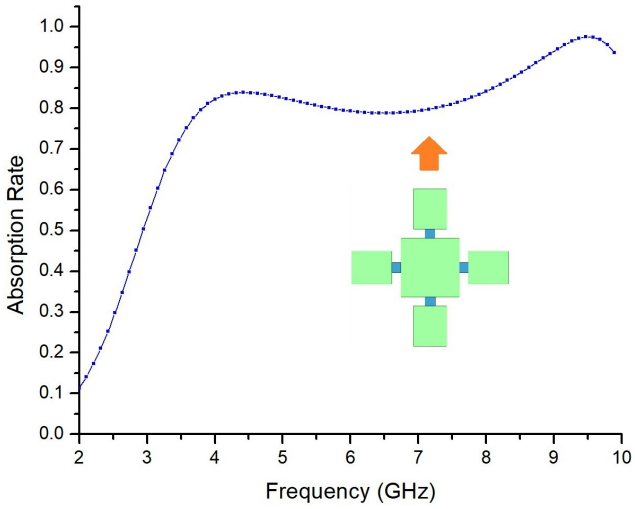

Figure 4. Absorption rate vs. frequency without multiple length of current.

intrinsic impedance in operating bandwidth.

Further, it has been observed that a wider bandwidth is achieved at the cost of absorption rate around 0.8 by removing the slotted configuration and replacing the octagonal structure with a square structure. In the proposed structure, it has been analyzed in Fig. 4. However, the enhancement of bandwidth with an absorption rate of 0.9 is observed with an octagonal structure and slotted parasitic elements. The absorption rate for the proposed CMMA for multiple resistor values is shown in Fig. 5. The decrement in resistor values affects absorption rate while increment in resistor values causes a reduction in bandwidth. Zero resistance loses absorptivity. Thus, RLC circuit parameter sources absorption in the proposed structure in which the resistor is used to decide absorption rate while LC configuration determines the operating bandwidth of proposed structure. An optimized 100 Ω resistor is chosen for CMMA. Fig. 6(a) shows the effect of coupling capacitance by controlling the distance between two intermediate unit cells. Fig. 6(a) displays that an increasing distance between unit cells reduces the bandwidth of the proposed structure. The less coupling between unit cell reduces the capacitance of the overall structure, which increases the quality factor. The quality factor is inversely proportional to

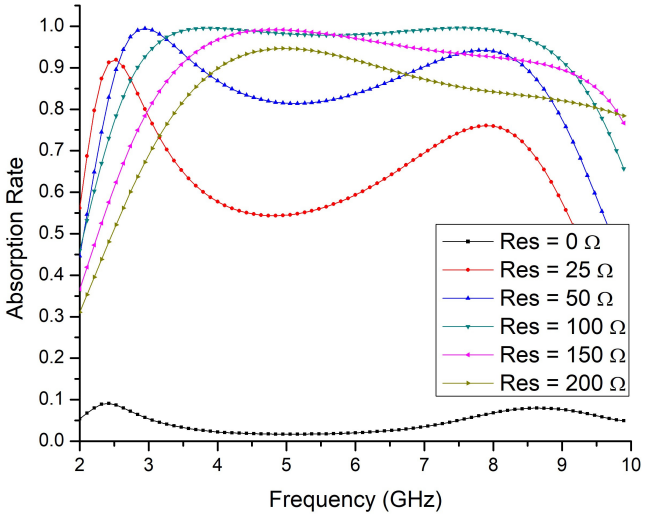

Figure 5. Absorption rate vs frequency with various resistor.

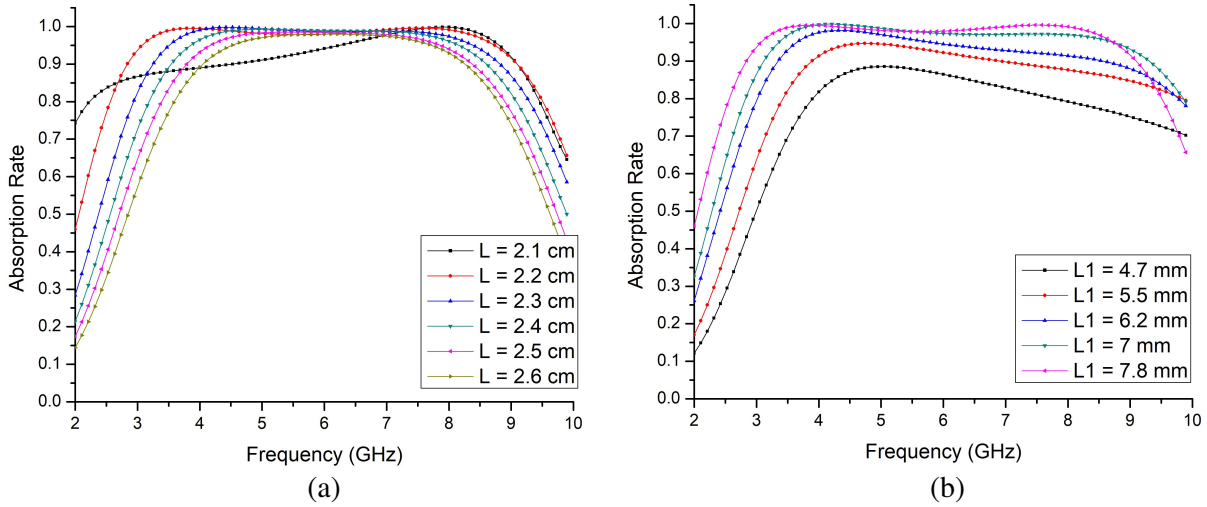

Figure 6. Absorption rate response for various (a) coupling capacitor, (b) variation of inductor value.

bandwidth which triggers reduction in bandwidth. The same can be analyzed from the value of $L = 2.3$ to 2.6 in Fig. 6(a). The structure at value $L = 2.1$ cm creates a tight coupling position, resulting in lower absorptivity at lower frequency as depicted in Fig. 6(a). Hence, the optimum value of this unit cell is 2.2 cm which is chosen for this structure.

Further, we can change the inductor value by controlling the current confinement in the proposed structure with the surface of structure variation, as shown in Fig. 6(b). Fig. 6(b) indicates that the decline in the surface of the proposed configuration causes an increase in the lowest frequency resulting in bandwidth drop. The theoretical reason for bandwidth reduction is that the inductor value depends on the current density of the proposed structure. As we decrease the exterior of configuration, its inductance value decreases, thus resulting in decrease in the current confinement, which results in a decrement in the bandwidth. After optimization, a 7.8 mm octagon has been chosen for the proposed structure. In light of the above evidence and analysis, the reason for absorption in wider bandwidth is multiple electrical lengths due to $L3$ and $L4$ with sufficient coupling between unit cells through C and resistor R to provide adequate absorption rate.

4. PARAMETRIC STUDY OBSERVATION

To observe the effect of physical and electrical parameters on absorption property, we have analyzed the CMMA structure by simulating variations. Fig. 7(a) shows shows the effect of thickness of the FR4 substrate with a constant air gap of 1 cm. It signifies that bandwidth is reduced from 105% to 95% of the proposed structure as we increase the substrate thickness. Desired outcome of bandwidth is achieved on 0.05 cm FR4 substrate. It is an easily available structure. Air gap is a mandatory parameter for enhancing the bandwidth; the same can be ascertained from Fig. 7(b), which shows that increment in the height of air gap increases the absorption rate over a broad bandwidth. The reason for the increase in bandwidth is the thickness of the overall structure having low effective dielectric constant, causing more substantial wave confinement, which results in matching the network, resulting in increased bandwidth. The optimum air gap chosen for this proposed structure is 1 cm.

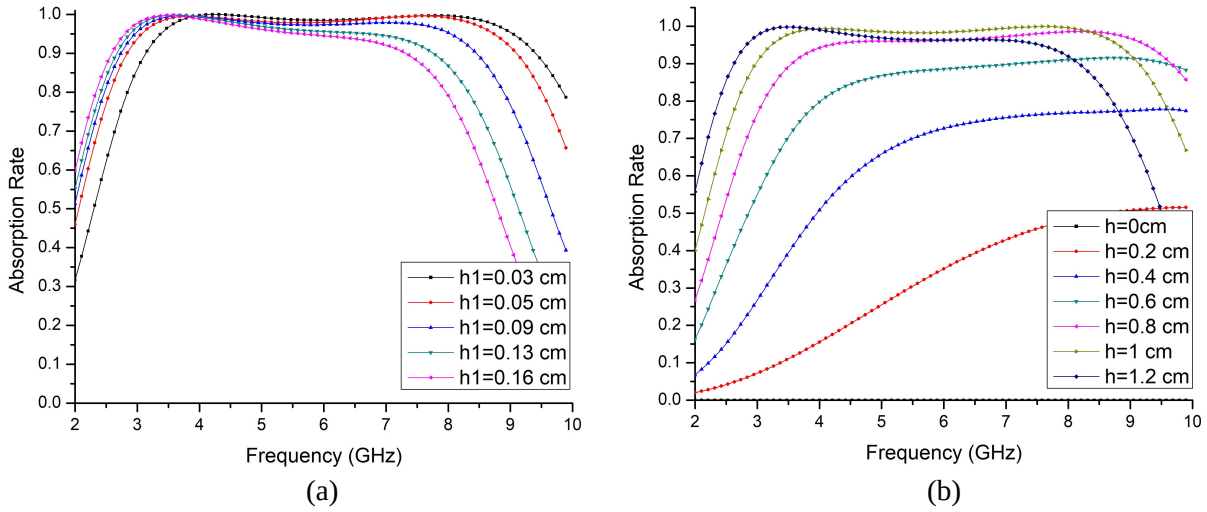

Figure 7. Absorption rate response for various (a) substrate thickness, (b) air gap variation.

Furthermore, from the analysis point of view, the effect of a dielectric constant is shown in Fig. 8(a). From Fig. 8(a), as we increase the dielectric constant, bandwidth increment does not give considerable variation because of the lower thickness of substrate material. The relative dielectric constant of 4.4 has been chosen for the proposed structure for practical implementation. The effect of loss tangent ($\tan\delta$) varying from 0 to 1 on the CMMA structure can be analyzed in Fig. 8(b). This indicates that as we increase the loss tangent, the lower cutoff frequency of the proposed structure decreases, which shows that the dissipation factor reduces the electric field components of the proposed configuration. From the parametric study, we can conclude that substrate height will be increased by including the air gap with a lower loss tangent for the betterment of bandwidth. The variation of various θ planes with a fixed ϕ plane is shown in Fig. 9 under TE and TM configurations after optimizing CMMA. The electric field vector and magnetic field vector consist of the same phase to the surface of CMMA in TM and TE, respectively. The proposed structure is oblique angle independent up to 30° in TE and TM configurations from 2.84 GHz to 9.12 GHz as shown in Fig. 9.

Table 1 shows the comparative study of proposed structure with the recently reported absorber. It indicates that the proposed structure absorbs a complete C band with a miniaturized structure in size and thickness. It has been observed that structure [33] includes C, X as well as Ku band, but it was designed by Indium tin oxide (ITO) resistive layers on adaptable polymer, whereas structure [36] based on multimode resistor — embedded metallic strips consisting of 8 resistors with two distinct values in the unit cell thereby increasing the complexity and fabrication cost on both of these structures as compared to the proposed structure. Theoretical and simulated results of a lossy surface without measurement outcome have been presented in structure [35]. So, the proposed CMMA is a practically cost-effective

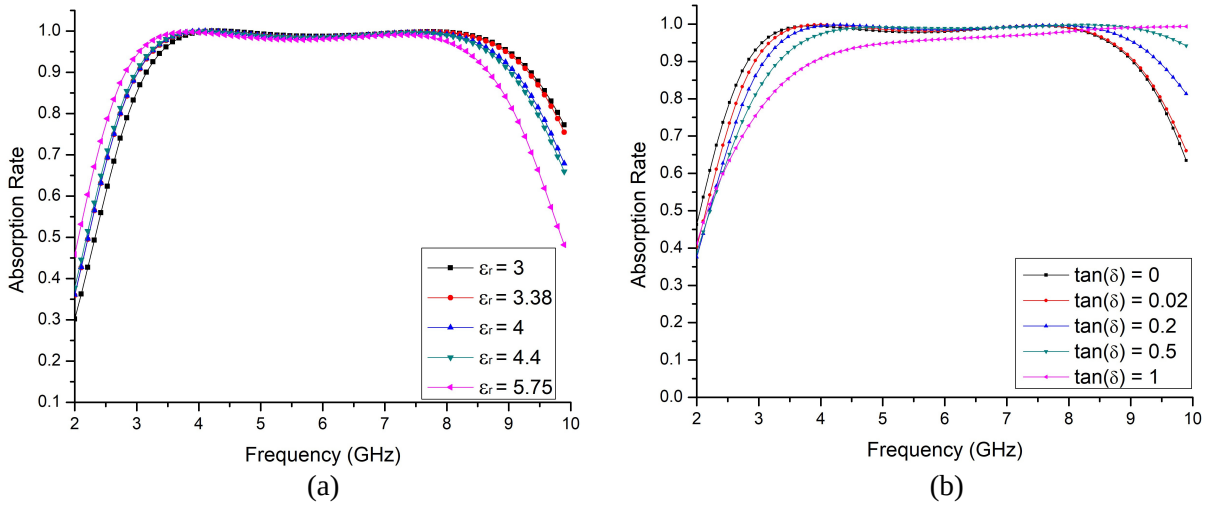

Figure 8. Absorption rate response for various (a) dielectric constant, (b) loss tangent.

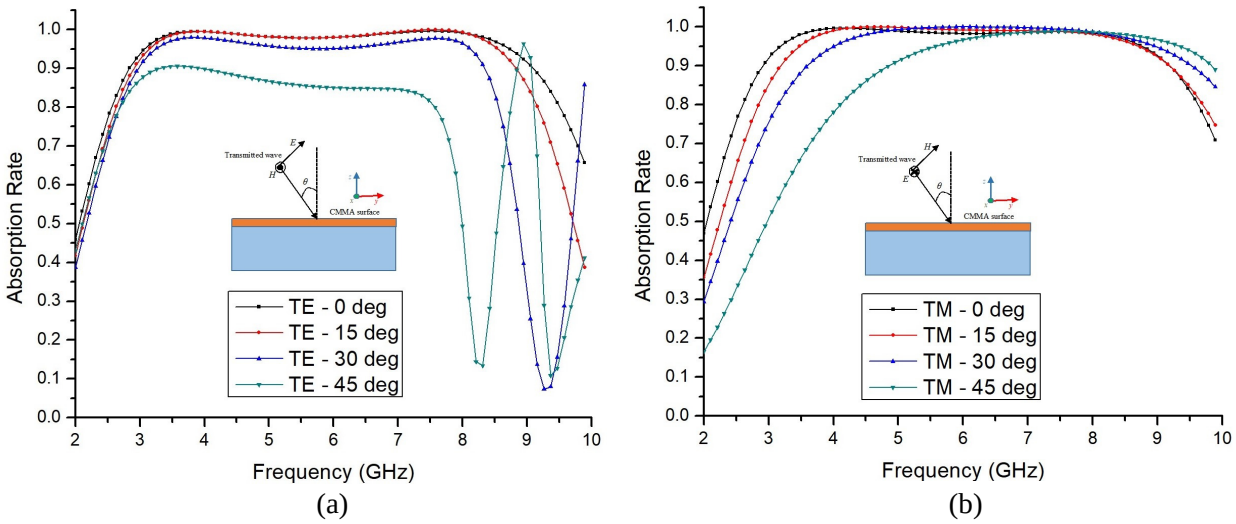

Figure 9. Absorption rate for various oblique angle incidence (a) TE configuration, (b) TM configuration.

novel solution to design the RF harvesting circuits as well as stealth application by absorbing the entire C band with miniaturization.

5. EXPERIMENTAL VERIFICATION OF FABRICATED STRUCTURE

The proposed CMMA structure has been fabricated on a 0.5 mm FR4 substrate with 1 cm air gap. This structure consists of 12×12 octagon-shaped unit cells to establish a metamaterial structure (size — 26.4 cm $\times$ 26.4 cm) as shown in Fig. 10. The return loss S_{11} can be used to calculate the absorptivity of CMMA structure from a wideband horn antenna connected to the Anritsu vector network analyzer (MS 2037C) ranging from 9 kHz to 15 GHz in the anechoic chamber, as shown in Fig. 11. The absorption rate was evaluated by the difference of return loss S_{11} measured from the perfect electric conductor with the same size of CMMA and return loss S_{11} measured from the complete CMMA structure at the

Table 1. Comparison between CMMA with the existing structure.

Absorber	Cut off frequency (GHz)	Frequencies (GHz)	Fractional Bandwidth	Periodicity (mm)	Thickness (mm)	Oblique angle insensitive (TE and TM)
Marathe D. et al. [23]	11.32	8.89 to 13.83	44.35%	$5(0.15\lambda_H)$	$1.6(0.05\lambda_H)$	Up to 20°
G. W. Zhang et al. [26]	1.87	1 to 2.74	93%	$20(0.067\lambda_H)$	$23(0.078\lambda_H)$	Up to 30°
H. Sheokand et al. [33]	10.6	4 to 17.20	124.53%	$16.2(0.22\lambda_H)$	$6(0.8\lambda_H)$	Up to 30°
M. Bağmancı et al. [34]	9.85	6.8 to 12.8	121.83%	$12(0.272\lambda_H)$	$3.2(0.73\lambda_H)$	Up to 45°
B. Doken et al. [35]	4.3	2 to 6.6	107%	$26.2(0.174\lambda_H)$	$10(0.08\lambda_H)$	Up to 30°
B. Zhang et al. [36]	7.435	2.68 to 12.19	127.9%	$22.5(0.2\lambda_H)$	$10(0.08\lambda_H)$	Up to 30°
Proposed	5.98	2.84 to 9.12	105%	$22(0.15\lambda_H)$	$15(0.3\lambda_H)$	Up to 30°

receiver end. Fig. 12 shows the measurement result, which signifies that proposed structure is operated in the frequency range of 2.1 GHz to 8.8 GHz (123%). Measurement error may be because of the lossy dielectric substrate as well as tolerance of lumped resistors in fabrication.

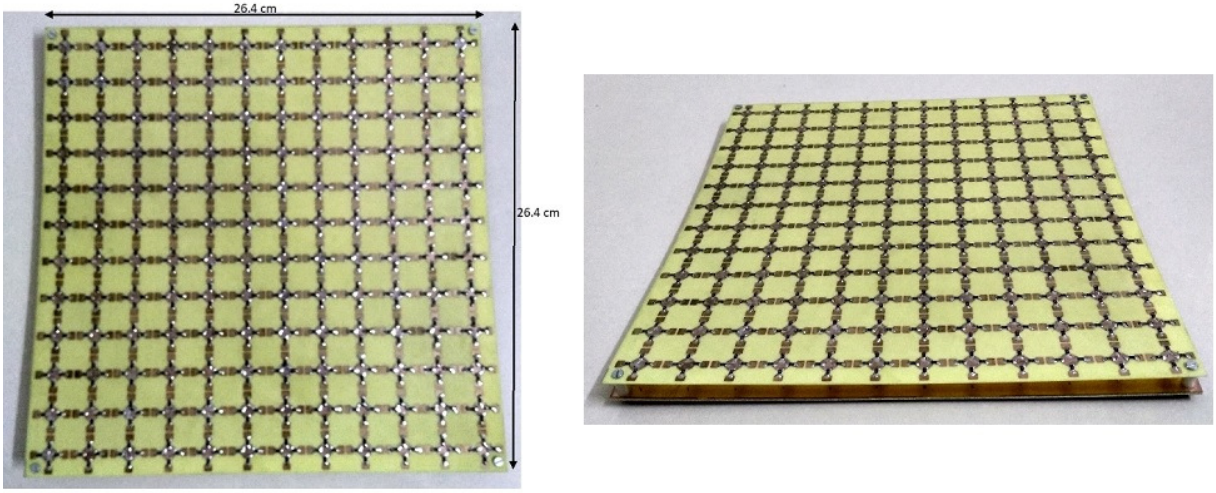

Figure 10. Front and side view of proposed fabricated CMMA structure.

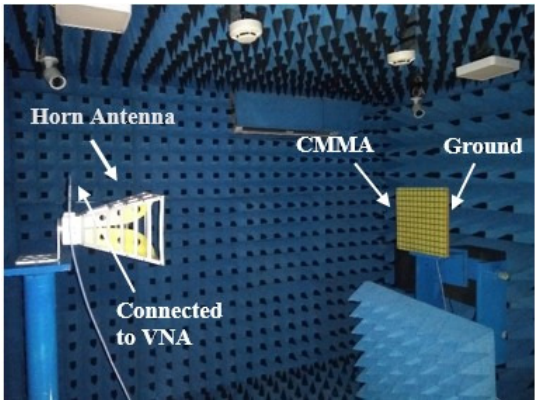

Figure 11. Measurement verification of CMMA structure.

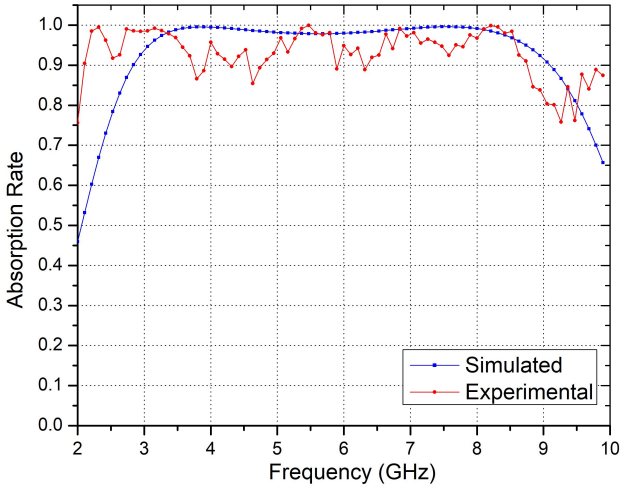

Figure 12. Measurement result compared with simulated result of CMMA.

6. CONCLUSIONS

In this paper, a wideband polarization-independent structure is designed and measured in an anechoic chamber. The bandwidth of the fabricated proposed configuration was 2.1 GHz to 8.8 GHz, which is nearly the same as simulated structure 2.84 GHz to 9.12 GHz, hence it can be widely used to absorb complete C band. It operates in C band with TE and TM configurations to achieve the polarization-independent structure. This structure also has novelty of miniaturization to 0.15λ and 0.30λ in size and thickness, respectively. Hence, in light of the above results and observation, it can be concluded that the proposed CMMA structure is applicable to stealth technology as well as RF harvesting structure to operate in a low power sensor network.

ACKNOWLEDGMENT

The research was performed and carried out at the ELARC — ELectromagnetics and Antenna Research Centre, which is operated for BVM Engineering College, Vallabh Vidya Nagar (Gujarat)-India by Electronics Engineering department.

REFERENCES

1. Veselago, V. G., "The electrodynamics of substances with simultaneously negative values of ϵ and μ," *Soviet Physics Uspekhi*, Vol. 10, No. 4, 509, 1968.
2. Landy, N. I., S. Sajuyigbe, J. J. Mock, D. R. Smith, and W. J. Padilla, "Perfect metamaterial absorber," *Physical Review Letters*, Vol. 100, No. 20, 1–4, 2008, ISSN: 00319007.
3. Schurig, D., J. J. Mock, and D. R. Smith, "Electric-field-coupled resonators for negative permittivity metamaterials," *Applied Physics Letters*, Vol. 88, No. 4, 1–3, 2006, ISSN: 00036951.
4. Palandoken, M., "Microstrip antenna with compact anti-spiral slot resonator for 2.4 GHz energy harvesting applications," *Microwave and Optical Technology Letters*, Vol. 58, No. 6, 1404–1408, 2016, ISSN: 10982760.
5. Wang, Y., T. Sun, T. Paudel, Y. Zhang, Z. Ren, and K. Kempa, "Metamaterial plasmonic absorber structure for high efficiency amorphous silicon solar cells," *Nano Letters*, Vol. 12, 440–445, 2012.
6. Costa, F., S. Genovesi, and A. Monorchio, "A chipless RFID based on multiresonant high-impedance surfaces," *IEEE Transactions on Microwave Theory and Techniques*, Vol. 61, No. 1, 146–153, 2012, ISSN: 15579670.

7. Chakradhary, V. K., et al., "Design of frequency selective surface-based hybrid nanocomposite absorber for stealth applications," *IEEE Transactions on Microwave Theory and Techniques*, Vol. 66, No. 11, 4737–4744, 2018, ISSN: 15579670.
8. Sheng, X., et al., "Transmissive/reflective frequency selective surface for satellite applications," *IEEE Antennas and Wireless Propagation Letters*, Vol. 17, No. 7, 1136–1140, 2018, ISSN: 15485757.
9. Kim, Y. J., Y. J. Yoo, K. W. Kim, J. Y. Rhee, Y. H. Kim, and Y. Lee, "Dual broadband metamaterial absorber," *Optics Express*, Vol. 23, No. 4, 3861–3868, 2015, ISSN: 10944087.
10. Gao, M., S. M. A. M. H. Abadi, and N. Behdad, "A dual-band, inductively coupled miniaturized-element frequency selective surface with higher order bandpass response," *IEEE Transactions on Antennas and Propagation*, Vol. 64, No. 8, 3729–3734, 2015, ISSN: 15582221.
11. Kaur, K. P., T. K. Upadhyaya, and M. Palandoken, "Dual-band polarization-insensitive metamaterial inspired microwave absorber for LTE-band applications," *Progress In Electromagnetics Research C*, Vol. 77, 91–100, 2017.
12. Kaur, K. P. and T. K. Upadhyaya, "Performance evaluation of wide-angle ultrathin microwave metamaterial absorber with polarization independence," *Advanced Electromagnetics*, Vol. 7, 71–77, 2018.
13. Mishra, N., K. Kumari, and R. K. Chaudhary, "A dual resonator-based polarisation-independent dual-band metamaterial absorber," *International Journal of Electronics Letters*, Vol. 7, 338–351, 2019.
14. Bhattacharyya, S., S. Ghosh, and K. Vaibhav Srivastava, "Triple band polarization-independent metamaterial absorber with bandwidth enhancement at X-band," *Journal of Applied Physics*, Vol. 114, No. 9, 2013.
15. Wang, G.-D., J.-F. Chen, X. Hu, Z.-Q. Chen, and M. Liu, "Polarization-insensitive triple-band microwave metamaterial absorber based on rotated square rings," *Progress In Electromagnetics Research*, Vol. 145, 175–183, 2014.
16. Kartal, M., J. J. Golezani, and B. Doken, "A triple band frequency selective surface design for GSM systems by utilizing a novel synthetic resonator," *IEEE Transactions on Antennas and Propagation*, Vol. 65, No. 5, 2724–2727, 2017.
17. Mei, P., S. Zhang, X. Q. Lin, and G. F. Pedersen, "A triple-band absorber with wide absorption bandwidths using an impedance matching theory," *IEEE Antennas and Wireless Propagation Letters*, Vol. 18, No. 3, 521–525, 2019.
18. Bathani, N. J. and J. M. Rathod, "Analysis of conformal quad band metamaterial absorber design on planar and cylindrical surface," *Progress In Electromagnetics Research M*, Vol. 103, 37–47, 2021.
19. Wang, B. X., X. Zhai, G. Z. Wang, W. Q. Huang, and L. L. Wang, "Design of a four-band and polarization-insensitive terahertz metamaterial absorber," *IEEE Photonics Journal*, Vol. 7, No. 1, 1–8, 2015.
20. Ranjan, P., C. Barde, A. Choubey, R. Sinha, A. Jain, and K. Roy, "A wideband metamaterial cross polarizer conversion for C and X band applications," *Frequenz*, 2021.
21. Lan, J., X. Cao, J. Gao, L. Cong, S. Wang, and H. Yang, "Design of miniaturized wideband microwave absorber loaded with lumped resistance," *Radioengineering*, Vol. 27, No. 3, 746–752, 2018, ISSN: 1805-9600.
22. Li, B. and Z. Shen, "Wideband 3D frequency selective rasorber," *IEEE Transactions on Antennas and Propagation*, Vol. 62, No. 12, 6536–6541, 2014.
23. Marathe, D. and K. A. Kulat, "A wideband wide-angle ultrathin low profile metamaterial microwave absorber," *Microwave and Optical Technology Letters*, Vol. 60, No. 3, 799–801, 2018, ISSN: 10982760.
24. Ranjan, P., A. Choubey, S. K. Mahto, R. Sinha, and C. Barde, "A novel ultrathin wideband metamaterial absorber for X-band applications," *Journal of Electromagnetic Waves and Applications*, Vol. 33, No. 17, 2341–2353, 2019.
25. Barde, C., A. Choubey, and R. Sinha, "Wide band metamaterial absorber for Ku and K band applications," *Journal of Applied Physics*, Vol. 126, No. 17, 175104, 2019.

26. Zhang, G. W., J. Gao, X. Y. Cao, S. J. Li, and H. H. Yang, "Wideband miniaturized metamaterial absorber covering L-frequency range," *Radioengineering*, Vol. 27, No. 1, 154–160, 2019, ISSN: 1805-9600.
27. Barde, C., A. Choubey, R. Sinha, et al., "A compact wideband metamaterial absorber for Ku band applications," *Journal of Materials Science: Materials in Electronics*, Vol. 31, No. 19, 16898–16906, 2020.
28. Dincer, F., O. Akgol, M. Karaaslan, E. Unal, and C. Sabah, "Polarization angle independent perfect metamaterial absorbers for solar cell applications in the microwave, infrared, and visible regim," *Progress In Electromagnetics Research*, Vol. 144, 93–101, 2014.
29. Sun, H., "Broadband and broad-angle polarization-independent metasurface for radar cross section reduction," *Scientific Reports*, Vol. 7, No. 1, 1–9, 2017.
30. Han, Y., W. Che, X. Xiu, W. Yang, and C. Christopoulos, "Switchable low-profile broadband frequency-selective rasorber/absorber based on slot arrays," *IEEE Transactions on Antennas and Propagation*, Vol. 65, No. 12, 6998–7008, 2017.
31. Li, H., F. Costa, Y. Wang, Q. Cao, and A. Monorchio, "A wideband and polarization-insensitive switchable absorber/reflector with simple biasing configuration," *IEEE International Conference on Computational Electromagnetics ICCEM*, 1–3, 2019.
32. Kiani, G. I., A. R. Weily, and K. P. Essell, "Frequency selective surface absorber using resistive cross-dipoles," *IEEE Antennas and Propagation Society International Symposium*, 4199–4202, 2006.
33. Sheokand, H., G. Singh, S. Ghosh, J. Ramkumar, S. A. Ramakrishna, and K. V. Srivastava, "An optically transparent broadband microwave absorber using interdigital capacitance," *IEEE Antennas and Wireless Propagation Letters*, Vol. 18, No. 1, 113–117, 2019.
34. Bağmancı, M., O. Akgöl, M. Özaktürk, M. Karaaslan, E. Ünal, and M. Bakır, "Polarization independent broadband metamaterial absorber for microwave applications," *International Journal of RF and Microwave Computer-Aided Engineering*, Vol. 29, No. 1, 1–10, 2019.
35. Doken, B., M. Kartal, and S. Balta, "A simple frequency selective absorber surface design," *9th International Conference on Recent Advances in Space Technologies (RAST)*, 79–82, IEEE, 2019.
36. Zhang, B., C. Jin, and Z. Shen, "Low-profile broadband absorber based on multimode resistor-embedded metallic strips," *IEEE Transactions on Microwave Theory and Techniques*, Vol. 68, No. 3, 835–843, 2020, ISSN: 15579670.